

# Quantitative characterization of higher-order mode converters in weakly multimoded fibers

M. Skorobogatiy\*

*Ecole Polytechnique de Montréal, Génie Physique, C.P. 6079, succ. Centre-Ville Montréal,  
Quebec H3C3A7, Canada*

[maksim.skorobogatiy@polymtl.ca](mailto:maksim.skorobogatiy@polymtl.ca)

**Charalambos Anastassiou\*, Steven G. Johnson\*, O. Weisberg,  
Torkel D. Engeness, Steven A. Jacobs, Rokan U. Ahmad, Yoel Fink**

*OmniGuide Communications, One Kendall Square, Build. 100, Cambridge, MA 02139, USA*

*\*These authors contributed equally to the paper.*

**Abstract:** We present a rigorous analysis methodology of fundamental to higher order mode converters in step index few mode optical fibers. We demonstrate experimental conversion from a fundamental  $LP_{01}$  mode to the higher order  $LP_{11}$  mode utilizing a multiple mechanical bend mode converter. We perform a quantitative analysis of the measured light intensity, and demonstrate a modal decomposition algorithm to characterize the modal content excited in the fiber. Theoretical modelling of the current mode converter is then performed and compared with experimental findings.

© 2003 Optical Society of America

**OCIS codes:** (060.2340) Fiber optics components; (060.2300) Fiber measurements

---

## References and links

1. Y. Danziger and D. Askegard, "Full Fiber Capacity Realized with High Order Mode Technology," in *IEC Annual Review*, (2000).
2. Kerbage C, Windeler RS, Eggleton BJ, Mach P, Dolinski M and Rogers JA, "Tunable devices based on dynamic positioning of micro-fluids in micro-structured optical fiber," *Opt. Commun.* **204**, 179 (2002).
3. Steven G. Johnson, Mihai Ibanescu, M. Skorobogatiy, Ori Weisberg, Torkel D. Engeness, Marin Soljačić, Steven A. Jacobs, J. D. Joannopoulos and Yoel Fink, "Low-loss asymptotically single-mode propagation in large-core OmniGuide fibers," *Opt. Express* **9**, 748 (2001), <http://www.opticsexpress.org/abstract.cfm?URI=OPEX-9-13-748>
4. R.C. Youngquist, J.L. Brooks and H.J. Shaw, "Two-mode fiber modal coupler," *Opt. Lett.* **9**, 177 (1984).
5. J. L. Brooks, R. C. Youngquist and G. S. Kino "Active polarization coupler for birefringent fiber," *Opt. Lett.* **9**, 249 (1984).
6. W P. Risk, R. C. Youngquist and G. S. Kino "Acousto-optic frequency shifting in birefringent fiber," *Opt. Lett.* **9**, 309 (1984).
7. J.N. Blake, B.Y. Kim and H.J.Shaw, "Fiber-optic modal coupler using periodic microbending," *Opt. Lett.* **11**, 177 (1986).
8. K.O. Hill, B. Malo, K.A. Vineberg, F. Bilodeau, D.C. Johnson and L. Skinner, "Efficient mode conversion in telecommunication fibre using externally written gratings," *Electronics Lett.* **26**, 1270 (1990).
9. C.D. Poole, C.D. Townsend and K.T. Nelson, "Helical-grating two-mode fiber spatial-mode coupler," *J. Lightwave Techn.* **9**, 598 (1991).
10. K.S. Lee and T. Erdogan, "Fiber mode conversion with tilted gratings in an optical fiber," *J. Opt. Soc. Am. A* **18**, 1176 (2001).
11. K.S. Lee, "Coupling analysis of spiral fiber gratings," *Opt. Commun.* **198**, 317 (2001).
12. A.A. Ishaaya, G. Machavariani, N. Davidson, A.A. Friesem and E. Hasman "Conversion of a high-order mode beam into a nearly Gaussian beam by use of a single interferometric element," *Opt. Lett.* **28**, 504 (2003).
13. P. Yeh, A. Yariv and E. Marom, "Theory of Bragg fiber," *J. Opt. Soc. Am. A* **68**, 1196–1201 (1978).
14. A.J. Fielding, K. Edinger and C.C. Davis, "Experimental Observation of Mode Evolution in Single-Mode Tapered Optical Fibers," *J. Lightwave Techn.* **17**, 1649 (1999).

15. M. Skorobogatiy, Steven A. Jacobs, Steven G. Johnson and Yoel Fink, "Geometric variations in high index-contrast waveguides, coupled mode theory in curvilinear coordinates," *Opt. Express* **10**, 1227 (2002), <http://www.opticsexpress.org/abstract.cfm?URI=OPEX-10-21-1227>
  16. B. Z. Katsenelenbaum, L. Mercader del Río, M. Pereyaslavets, M. Sorolla Ayza and M. Thumm, *Theory of Nonuniform Waveguides: The Cross-Section Method* (Inst. of Electrical Engineers, London, 1998)
- 

## 1. Introduction

Conversion from fundamental to the higher-order modes in optical fiber has received a considerable interest due to potential applications in dispersion compensation, variable attenuation, and enhanced transmission properties [1–3]. Many schemes have been proposed to perform fundamental to higher-order mode conversion including fiber bends, long-period fiber Bragg gratings, tapers of various topologies, and phase masks [4–12]. While many experiments demonstrating mode conversion have been described, few of them were subjected to a rigorous analysis of the intensity plots and a comparison with theoretical predictions. Typical uncertainties in the modal weights from these experiments can reach tens of percents. The aim of this paper is to present a rigorous analysis methodology for fundamental to higher-order mode converters and to discuss inherent limitations of such an analysis.

Devising such a methodology relies on several key capabilities. One is to perform modal decomposition of the intensity plots into the constituent modes of a fiber. As phase information is absent from the intensity plots, the problem of fitting the modal content of the multimode fiber is generally ill-conditioned. In low index-contrast fibers, one can successfully perform modal decomposition of intensity plots only into the *LP* modal groups rather than into the individual modes. Another challenging task is to simulate the components of the imaging setup as precisely as possible to achieve smaller than a few percent accuracy in prediction of the true modal weights. Part of the uncertainty of any theoretical simulation comes from an uncertainty of the fiber specifications, which are usually known only to several percent. Another uncertainty comes from the limited knowledge of the experimental setup parameters, such as the precise fiber center-line deviation in a bent fiber. Therefore, if quantitative comparison with experimental data is desired, the experiment has to be designed around these uncertainties.

In this paper, we devise a self-consistent experimental-theoretical methodology that allows the quantitative characterization of fundamental to higher-order mode converters. Our paper is organized as follows. We first describe a particular type of mode converter used in our experiments, which is based on multiple fiber bends. Then, experimental setup and results are discussed. After that, a novel modal characterization algorithm is presented, experimental data is analyzed, and the modal weights of different *LP* modes are extracted. Finally, we perform theoretical modelling of mode conversion and compare its results with weights fitted by the modal characterization algorithm.

## 2. Serpentine mode converter, design and experimental setup

"Serpentine" mode converters based on multiple single-plane bends of an optical fiber have been described in many papers [7, 9, 11]. Single in-plane bend can directly couple modes with angular indexes different by  $\Delta m = 1$ . Such a bend couples differently modes with polarizations in the plane of the bend and modes with polarizations perpendicular to the plane, without mixing between polarizations. Coupling between modes is stronger, the larger is the curvature of a bend. Periodic ("serpentine") bends with spatial period  $\Lambda$ , in addition, induce a phase matching condition that preferentially couples the modes with propagation constants different by  $|\Delta\beta| = \frac{2\pi}{\Lambda}$ . This allows a selective higher-order mode excitation. A typical "serpentine" mode converter (Fig. 1) consists of two sets of tightly wound wires of diameter  $D_w$  with an optical fiber of outer diameter  $D_f$  placed between them. When the upper wires are pressed down,

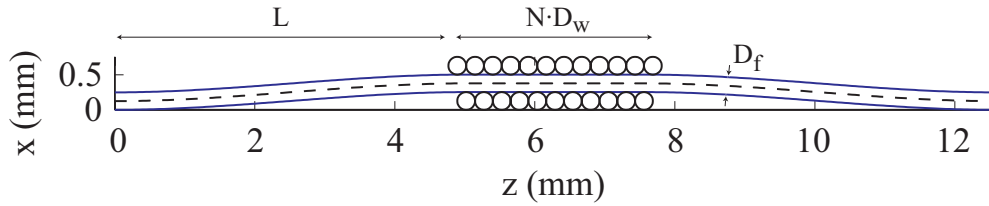


Fig. 1. Serpentine mode converter geometry. Optical fiber is in-between the two sets of tightly wound wires of diameter  $D_w$ , chosen to satisfy phase matching condition between the converted modes. Fiber diameter  $D_f$  is generally comparable to the  $D_w$ .

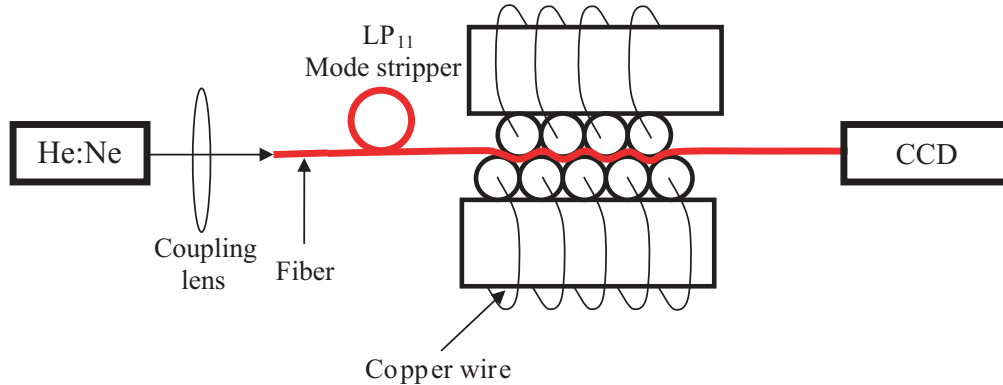


Fig. 2. Schematic of an experimental setup. Light from *He : Ne* laser, is coupled into the fiber through the coupling lens. A mode stripper is then applied consisting of several loops of tightly wound fiber. The wire wrapped mandrel on *xyz* stage was used as a mode converter with fiber squeezed between two wire sets. The far field images were captured with a CCD camera placed  $13\text{mm}$  from the fiber end.

they induce a periodic sequence of mechanical bends in the fiber. By choosing the diameter of the wires  $D_w$  to satisfy the phase-matching condition between the target modes of a fiber, one can achieve mode conversion between them. If  $N$  is the number of wire loops, then the length of the coupler is  $N \cdot D_w$ . When entering and exiting the coupler, the fiber is glued to a substrate at some distance  $L$  from a converter, chosen in such a way as to not induce additional modal conversion in these interface regions.

In our experiments, we perform an  $LP_{01}$  to  $LP_{11}$  mode conversion in *SMF-28* and *SM-750* fibers operating at  $\lambda = 632.8\text{nm}$ .  $LP_{01}$  is a singlet  $HE_{11}$  gaussian-like mode with propagation constant  $\beta_{LP_{01}}$  and  $LP_{11}$  is a triplet of  $TE_{01}$ ,  $TM_{01}$ ,  $HE_{21}$  modes with almost degenerate propagation constants  $\beta_{LP_{11}}$ . Modes in each *LP* group exhibit very similar intensity patterns, but not the field patterns. Vector fields are very different for different modes in the same *LP* group, reflecting correspondent modal symmetries. The coupler resonant condition is therefore  $D_w = \frac{2\pi}{|\beta_{LP_{01}} - \beta_{LP_{11}}|}$  which for *SMF-28* is  $D_w = 0.519\mu\text{m}$ , and for *SM-750* is  $D_w = 0.246\mu\text{m}$ .

A schematic of the experimental setup is shown in Fig. 2. Light with  $\lambda = 632.8\text{nm}$  from a He:Ne laser is coupled into the fiber, exciting mostly the  $LP_{01}$  mode of the fiber. This is achieved by first collimating the laser beam to  $1\text{cm}$  and then focusing it into the fiber with a lens of focal length  $8.3\text{cm}$  and  $3.8\text{cm}$  for the *SMF-28* and the *SM-750* respectively. A mode stripper is then applied to ensure that any higher order modes excited are stripped and only the  $LP_{01}$  mode is sent to the mode converter. The mode stripper consisted of three loops of  $6\text{mm}$  diameter

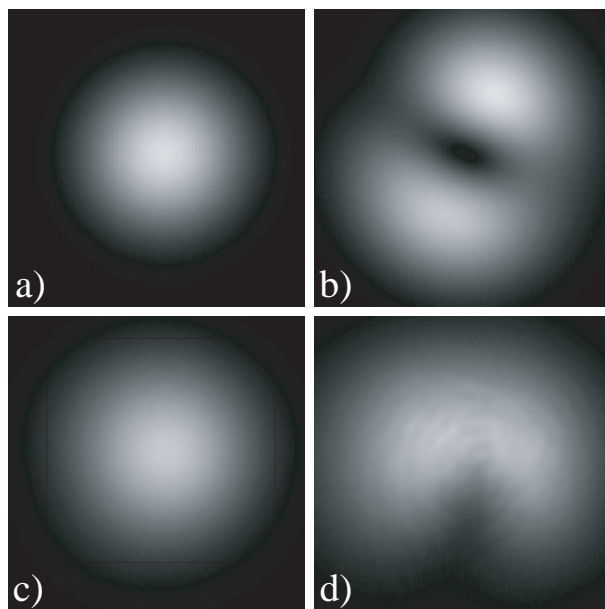


Fig. 3. Far field images taken 13 mm from exit of *SMF* – 28 (a) and (b) and *SM* – 750 (c) and (d) being excited with He:Ne. (a) No mode converter applied for *SMF* – 28 showing the  $LP_{01}$ . (b) Mode converter applied with  $N = 35$  turns of 0.512 mm copper wires showing 65% conversion to  $LP_{11}$  (established by modal characterization algorithm). (c) No mode converter applied for *SM* – 750 showing the  $LP_{01}$  mode. (d) Mode converter applied with  $N = 14$  turns of 0.254 mm copper wires showing 55% conversion to  $LP_{11}$  (established by modal characterization algorithm).

for the *SMF* – 28 and only one loop of 12.7 mm diameter for the *SM* – 750. The  $LP_{01}$  to  $LP_{11}$  mode converter, shown in Fig. 2, was built by wrapping two cylinders (12.7 mm diameter) with a copper wire and squeezing the fiber in between them. The copper wire diameter was chosen to be as close to the beat length of the two modes as possible. We used 0.512 mm and 0.254 mm wire diameters for the *SMF* – 28 and the *SM* – 750, respectively. The wire-wrapped mandrels were put on the xyz stages to adjust the amount of separation between the mandrels and their relative alignment and pressure applied to the fiber in order to achieve maximal conversion. Care was also taken to ensure there were no additional sharp bends after the mode converter, this was particularly critical for the *SM* – 750 due to the very high bending losses of its  $LP_{11}$  mode.

The far-field images shown in Fig. 3 were taken 13 mm away from the exit of the fibers, captured with a CCD camera (Cohu 4812) and a Spiricon LBA500-PC frame grabber. The CCD camera had its protective glass removed to prevent reflections from distorting the image. Fig. 3(a) and Fig. 3(b) show the image with no bend and with bend applied for maximum conversion for the *SMF* – 28; the corresponding images for the *SM* – 750 are shown in Fig. 3(c) and Fig. 3(d). All of the images were then decomposed into the corresponding fiber modes by using the modal characterization tool described in the following section. We thus found that the maximum  $LP_{01}$  to  $LP_{11}$  conversion is 65% in the case of *SMF* – 28 with  $N = 35$  wire turns, and 55% for the *SM* – 750 converters with  $N = 14$  wire turns.

Table 1 summarizes the experimental parameters and results. The fiber parameters were used in the spatial decomposition program and were taken from the manufacturer specifications. Specifications of fiber geometry usually allow up to 5% uncertainties in their values, while

the knowledge of the refractive index is somewhat better controlled. Uncertainties in the wire diameter can be up to 1%. Uncertainties of the modal characterization algorithm is 5%.

Table 1. Experimental parameters of fibers and wires including core diameter, core and cladding refractive indexes, wire diameter and  $LP_{01}$  to  $LP_{11}$  conversion efficiency

|        | $D_{core}$ ( $\mu\text{m}$ ) | $n_{core}$ | $n_{clad}$ | $D_w$ ( $\mu\text{m}$ ) | Conv. Eff. (%) |
|--------|------------------------------|------------|------------|-------------------------|----------------|
| SMF-28 | 8.2                          | 1.4625     | 1.4572     | 512                     | $65 \pm 3$     |
| SM-750 | 4.46                         | 1.4622     | 1.4572     | 254                     | $55 \pm 3$     |

### 3. Modal characterization algorithm

The object of modal characterization is to infer the fractional power (weight) in each guided mode (eigenmode) from the far-field intensity pattern captured by the CCD. To do this, we perform a least-squares fit of the measured  $I_{mes}(\rho, \theta)$  to predicted  $I(\rho, \theta)$  intensity, with the modal weights and phases as fit parameters. This involves several steps. First, the eigenmodes of the specified fiber profile are computed by a transfer-matrix method [13]. These modes are coupled to modes of air by matching boundary conditions, and are propagated to yield the theoretical field pattern of each mode as it would appear at the detector. Then, for any given modal weights and phases, the fields can be summed to yield the total intensity. We then define “objective function,” as integral over the difference squared in predicted and measured intensities over the area of the image. Objective function is then minimized by a variety of standard methods by varying weights and phases (see [14] for an algorithm where phases are not included in the optimization). Ideally, this should reduce the objective function to zero, at which point we would know the modal weights and phases exactly. In practice, we are only able to reduce the objective function to a finite value because of experimental uncertainties, and we therefore obtain the modal weights and phases with a certain degree of uncertainty. Moreover, from a single intensity image, this method does not distinguish between individual, nearly degenerate, modes of an  $LP$  modal group.

We tested several function minimization algorithms to reduce the value of objective function. As we mentioned earlier, fitting phases is generally more problematic than fitting weights as phase information is lost in the intensity plots. However, we found that standard multidimensional conjugate gradient (CG) minimization algorithm where weights and phases are treated on equal footing works very well in this problem. Another very efficient minimization method that worked somewhat faster than CG was multidimensional Newton method. Weights and phases were treated on equal footing, however, not all dimensions were used to find a new searched direction. We used SVD decomposition of the Hessian of an objective function to reduce degenerate subspaces.

To ensure consistency in the calculations, we always normalize both the observed and calculated modes so that their integrated intensity on the screen is unity. In order to compare the calculated modes to the real modes of the fiber, it is also important that the calculated modes and the real modes be centered at the same location, and we therefore need an accurate measure of the center of the fiber. We locate the center experimentally by first sending a white light signal through the fiber and determining the “center of mass” of this image. This “center of mass” gives a correct center determination, because white source is incoherent, and the image that the white light creates is cylindrically symmetrical without any finer structure to it.

We now describe in more detail the computation of the objective function, the sum of the squares of the difference in predicted and measured intensity, a calculation that we simplify

somewhat by the use of Fourier series. The predicted intensity is the  $z$  component of the real part of the Poynting vector of the summed modes. We define  $(E_\rho^{mj}(\rho), E_\theta^{mj}(\rho)) \exp(im\theta)$  and  $(H_\rho^{mj}(\rho), H_\theta^{mj}(\rho)) \exp(im\theta)$  to be the transverse components of the electromagnetic fields corresponding to the propagated eigenmode  $j$  of a fiber characterized by an angular index  $m$  and propagation constant in the fiber  $\beta_j$ . The total field is then

$$F_{\rho,\theta} = \sum_j F_{\rho,\theta}^{mj}(\rho) e^{im\theta} \cdot w_j \cdot e^{i\phi_j} \quad (1)$$

where  $w_i$  is the modal weight,  $\phi_i$  is the modal phase, and  $F_{\rho,\theta}^{mj}$  is a transverse component of the electric or magnetic field. The time average predicted intensity  $I(\rho, \theta)$  is then

$$I(\rho, \theta) = \frac{1}{4} (\vec{H}^* \times \vec{E} + \vec{H} \times \vec{E}^*)_z = \sum_{\Delta m} \left( \sum_{i,j,m_i-m_j=\Delta m} f_{ij}(\rho) \cdot \omega_i \cdot \omega_j \cdot e^{i(\phi_i-\phi_j)} \right) \cdot e^{i\Delta m\theta} \equiv \sum_{\Delta m} \tilde{I}(\Delta m, \rho) \cdot e^{i\Delta m\theta}, \quad (2)$$

where we introduced a cross-flux as

$$f_{ij}(\rho) = \frac{1}{4} (E_\rho^{m_i}(\rho) \cdot H_\theta^{*m_j}(\rho) - E_\theta^{m_i}(\rho) \cdot H_\rho^{*m_j}(\rho))_z. \quad (3)$$

We now introduce the Fourier transform of the measured intensity field  $I_{mes}(\rho, \theta)$  as

$$\tilde{I}_{mes}(\Delta m, \rho) = \frac{1}{2\pi} \int_0^{2\pi} I_{mes}(\rho, \theta) \cdot e^{-i\Delta m\theta} d\theta. \quad (4)$$

Objective function is defined as an integral of the square of the difference between the experimental intensity and fitted intensity, and can be further expressed as

$$O = \int \rho d\rho d\theta (I(\rho, \theta) - I_{mes}(\rho, \theta))^2 = \int \rho d\rho \sum_{\Delta m} (\tilde{I}(\Delta m, \rho) - \tilde{I}_{mes}(\Delta m, \rho)) \cdot (\tilde{I}(-\Delta m, \rho) - \tilde{I}_{mes}(-\Delta m, \rho)) \quad (5)$$

Substitution of the  $\tilde{I}(\Delta m, \rho)$  into the above equation gives

$$O = \sum_{\Delta m} \left( \sum_{i,j,m_i-m_j=\Delta m} \sum_{i',j',m_{i'}-m_{j'}=\Delta m} \left[ \int \rho d\rho f_{ij}(\rho) f_{i'j'}^*(\rho) \right] \omega_i \omega_j \omega_{j'} \omega_{i'} e^{i(\phi_i+\phi_{j'}-\phi_j-\phi_{i'})} \dots \right. \\ \left. - 2 \cdot \text{Re} \sum_{i,j,m_i-m_j=\Delta m} \left[ \int \rho d\rho f_{ij}(\rho) \tilde{I}_{mes}(\Delta m, \rho) \right] \omega_i \omega_j e^{i(\phi_i-\phi_j)} + \int \rho d\rho |\tilde{I}_{mes}(\Delta m, \rho)|^2 \right). \quad (6)$$

The advantage of this formulation is that we can evaluate the mode-specific integrals only once, and reuse them with any experimental intensity images. When the mode-specific integrals have been calculated, we can very quickly evaluate the objective function as a function of the modal weights and phases. Also, during objective function minimization, the workload of evaluating the objective function repeatedly for different modal weights and phases is small and we can thus rapidly minimize the objective function. Furthermore, the workload for the evaluation of each minimization step does not scale with the size/number of pixels of the CCD, only with the number of modes, which permits us to use a high image resolution.

#### 4. Theoretical modelling

In this section we verify mode conversion by theoretical modelling of an experimental setup. We then compare theoretical findings with results from modal characterization of the experimental

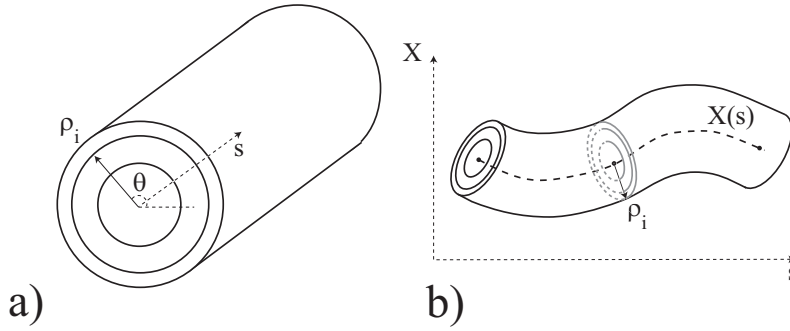


Fig. 4. (a) Dielectric profile of a cylindrically symmetric fiber. Concentric dielectric interfaces are characterized by their radii  $\rho_i$ . (b) Perturbations of a fiber center line in a 2D plane. Cross-section perpendicular to the fiber center line is assumed cylindrically symmetric, while the position of the fiber center is described by an analytic curve  $(X(s), s)$  confined to a plane.

intensity images. In our analysis, we employ a vectorial coupled mode theory developed for analysis of generic geometry variations of a fiber profile [15]. This formulation is also valid for high index-contrast fibers. For alternative formulations see also [16]. In particular, we simulate modal scattering in a fiber undergoing periodic mechanical bends assuming that initially all of the power is launched into the  $HE_{11}$  mode. Both linear polarizations are considered. We also assume that all the fiber bends are confined to a single plane.

Let  $(x, y, z)$  be the coordinates in a Cartesian coordinate system. In unperturbed, cylindrically symmetric, step-index fibers, the position of the dielectric interfaces can be described in cylindrical coordinates by a set of points  $(x = \rho \cos(\theta), y = \rho \sin(\theta), z = s)$ , where for the  $i$ -th dielectric interface  $\rho = \rho_i, \theta \in (0, 2\pi)$  (Fig. 4(a)). Now, consider perturbations of a fiber center line in a 2D plane. For such a perturbation, each cross-section perpendicular to the fiber center line remains cylindrically symmetric, while the position of the fiber center is described by an analytic curve confined to a plane. If  $(X(s), s)$  is an analytic curve in a 2D plane (see Fig. 4(b)), then the coordinate mapping

$$\begin{aligned} x &= X(s) + \rho \cos(\theta) \frac{1}{\sqrt{1 + (\frac{\partial X(s)}{\partial s})^2}} \\ y &= \rho \sin(\theta) \\ z &= s - \rho \cos(\theta) \frac{\frac{\partial X(s)}{\partial s}}{\sqrt{1 + (\frac{\partial X(s)}{\partial s})^2}}, \end{aligned} \quad (7)$$

will describe such a fiber center line perturbation. Here, as before,  $\rho = \rho_i, \theta \in (0, 2\pi)$  define the points on the  $i$ -th unperturbed dielectric interface, while the corresponding  $(x(\rho, \theta, s), y(\rho, \theta, s), z(\rho, \theta, s))$  describe the points on the perturbed interfaces, and  $s$  is chosen along one of the axes in a Cartesian coordinate system.

We choose a fiber center curve  $(X(s), s)$  to describe the features of a mode converter shown on Fig. 1 as follows. Input and output regions of the length  $L$  are described by elastic beam equations with a solution  $X^{i,o}(s) = \sum_{j=0}^3 A_j^{i,o} \cdot s^j$ , where the coefficients  $A_j^{i,o}$  are determined by zero-slope boundary conditions at the fixed points. In the converter region, the fiber center-line is described by a sinusoidal variation  $X(s) = D_w + \frac{D_f}{2} + \delta(\sin(2\pi \frac{s-s_0}{D_w}) - 1)$ , where  $\delta$  characterizes the strength of the perturbation. Parameters  $A_j^{i,o}$  and  $s_0$  are chosen to produce a continuous curve with continuous 1st and 2nd derivatives. For a fixed number of wire turns  $N$  and a transition length  $L$ , the parameter  $\delta$  is chosen to maximize the  $LP_{01}$  to  $LP_{11}$  conversion

for each of the polarizations.

As demonstrated in Ref. [15], modal scattering due to curving of the fiber center-line can be simulated in a coupled mode theory framework. Defining  $\vec{C}(s)$  to be the expansion coefficients into the unperturbed modes of a straight fiber, the following set of first order coupled differential equations have to be solved to find the weights of the excited modes

$$-iB \frac{\partial \vec{C}(s)}{\partial s} = M \vec{C}(s), \quad (8)$$

where  $B_{\beta^*, \beta'} = \frac{\beta'}{|\beta'|} \delta_{\beta, \beta'}$  is a normalization matrix, and  $M$  is a matrix of coupling elements given by

$$M_{\beta^*, m; \beta', m'} = \frac{\omega}{c} \int \rho d\rho d\theta \exp i(m' - m)\theta \times \begin{pmatrix} E_{\rho}^0(\rho) \\ E_{\theta}^0(\rho) \\ E_s^0(\rho) \\ H_{\rho}^0(\rho) \\ H_{\theta}^0(\rho) \\ H_s^0(\rho) \end{pmatrix}_{\beta^*}^{\dagger} \begin{pmatrix} \epsilon d_{\rho\rho} & \epsilon d_{\rho\theta} & \epsilon d_{\rho s} & 0 & 0 & 0 \\ \epsilon d_{\theta\rho} & \epsilon d_{\theta\theta} & \epsilon d_{\theta s} & 0 & 0 & 0 \\ \epsilon d_{s\rho} & \epsilon d_{s\theta} & \epsilon d_{s s} & 0 & 0 & 0 \\ 0 & 0 & 0 & d_{\rho\rho} & d_{\rho\theta} & d_{\rho s} \\ 0 & 0 & 0 & d_{\theta\rho} & d_{\theta\theta} & d_{\theta s} \\ 0 & 0 & 0 & d_{s\rho} & d_{s\theta} & d_{s s} \end{pmatrix} \begin{pmatrix} E_{\rho}^0(\rho) \\ E_{\theta}^0(\rho) \\ E_s^0(\rho) \\ H_{\rho}^0(\rho) \\ H_{\theta}^0(\rho) \\ H_s^0(\rho) \end{pmatrix}_{\beta'}^{m'}, \quad (9)$$

where the integration is performed over the unperturbed fields of a straight fiber. To the second order in  $\delta$ , the only non-zero elements of the coupling matrix are the ones corresponding to the  $|m' - m| = 1$  and  $|m' - m| = 0$  transitions. From Ref. [15] they are the following. For  $|m' - m| = 0$  non-zero coupling elements are calculated from 9 using  $-d_{ss} = d_{\rho\rho} = d_{\theta\theta} = \omega \frac{\delta^2}{2} \left( \frac{\partial X(s)}{\partial s} \right)^2$ . For  $|m' - m| = 1$  non-zero coupling elements are calculated from 9 using  $d_{ss} = -d_{\rho\rho} = -d_{\theta\theta} = \omega\rho \frac{\delta}{2} \frac{\partial^2 X(s)}{\partial s^2}$ . Equations (8) present a system of first order linear coupled differential equations with respect to a vector of expansion coefficients  $\vec{C}(s)$ . The boundary condition of a single incoming  $HE_{11}$  mode at the input of a converter defines a boundary value problem that can be solved numerically.

We now present the results of simulations for the two experimental implementations of a mode converter as described in the experimental setup section. The first experiment uses *SMF-28* optical fiber with four guided modal groups  $LP_{01}$ ,  $LP_{11}$ ,  $LP_{21}$ , and  $LP_{31}$ . Higher order modal groups  $LP_{11}$  and  $LP_{21}$  are both strongly coupled to the  $LP_{01}$  by bends. We calculated (and verified experimentally) that the length  $L$  of a coupling region should be at least 0.5 cm to avoid substantial mode scattering into the cladding due to bending at the converter input. In the experiment, we used  $L = 2$  cm,  $N = 35$  turns,  $D_w = 512 \mu\text{m}$ , and we find that the amplitude of fiber center-line oscillations to achieve the maximal  $LP_{01}$  to  $LP_{11}$  conversion for these parameters is  $\delta = 49$  nm. Fig. 5 presents the theoretical simulation of modal conversion in *SMF-28* fiber based converter at fixed  $\delta = 49$  nm as a function of the wire diameter  $D_w$ . Solid and dashed lines in Fig. 5 correspond to the input  $LP_{01}$  polarizations perpendicular and parallel to the plane of the converter, respectively. Upper two curves are the amplitudes (total of the squares of the modal weights) of the higher order  $LP_{11}$  group after conversion, while the lower two curves are the amplitudes of the original  $LP_{01}$  mode. The maximum conversion values are almost equivalent for both polarizations. Our simulations predict that, for a wire diameter  $D_w = 512 \mu\text{m}$ , the maximum conversion into  $LP_{11}$  is 80%—90% depending upon the state of the incoming polarization. This matches poorly with the maximal 65% conversion observed in analysis of experimental intensity images. Multiple reasons can account for such a discrepancy, including an uncertainty in the fiber parameters and the wire diameter. Note that a 1% deviation in the wire diameter from the experimental value  $512 \mu\text{m}$  changes the conversion rate from almost 100% to less than 60%, and the experimental radius was  $512 \pm 3 \mu\text{m}$ .

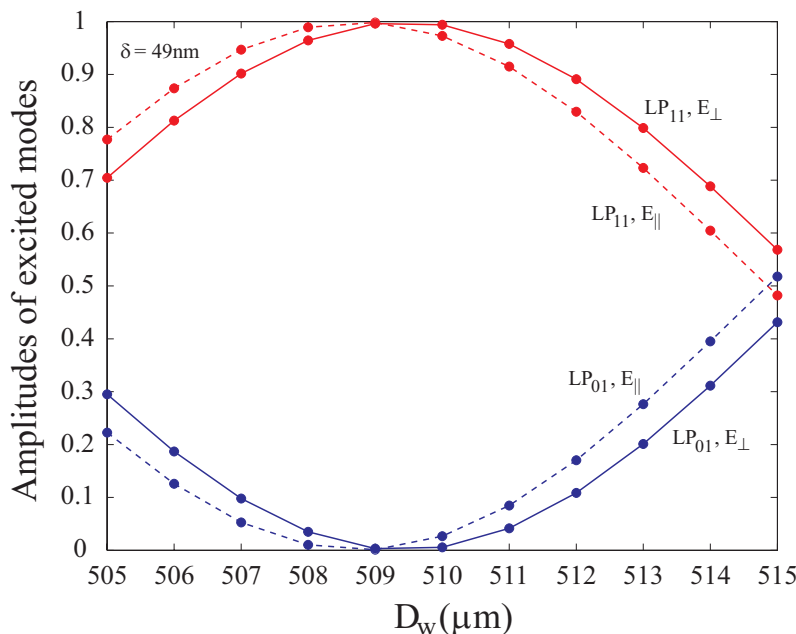


Fig. 5. Theoretical simulation of modal conversion as a function of a wire diameter in *SMF* – 28 fiber undergoing  $N = 35$  consecutive bends. Fiber centerline is described by a sinusoid with an amplitude of  $\delta = 49 \text{ nm}$  and a pitch equal to the wire diameter  $D_w$ . Solid and dashed lines correspond to the perpendicular and parallel to the plane of the converter polarizations of an incoming  $LP_{01}$  mode. Upper two curves correspond to the modal weights of the higher order  $LP_{11}$  group after conversion, while lower two curves correspond to the remaining weights of the original  $LP_{01}$  mode.

The second experiment uses *SM* – 750 optical fiber with only two guided modal groups,  $LP_{01}$  and  $LP_{11}$ . The higher order  $LP_{11}$  modes are very close to the cladding light line, and their losses increase dramatically with bending. We calculated (and verified experimentally) that the length  $L$  of a coupling region should be at least  $1 \text{ cm}$  to avoid substantial mode scattering into the cladding due to bending at the converter input. In the experiment we used  $L = 2 \text{ cm}$ ,  $N = 14$  turns,  $D_w = 254 \mu\text{m}$ , and we find that the amplitude of fiber center-line oscillations to achieve the maximal  $LP_{01}$  to  $LP_{11}$  conversion for these parameters is  $\delta = 110 \text{ nm}$ . Fig. 6 displays theoretical simulation of modal conversion in *SM* – 750 fiber based converter at fixed  $\delta = 110 \text{ nm}$  as a function of the wire diameter  $D_w$ . Like Fig. 5, solid and dashed lines correspond to perpendicular and parallel  $LP_{01}$  input, and the upper and lower curves are the output amplitudes of  $LP_{11}$  and  $LP_{01}$ . Note that scattering into cladding is stronger for the parallel polarization, so the maximum conversion rate for two polarizations is somewhat different because of the substantial radiation loss for the parallel polarization. Our simulations predict that for a wire diameter  $D_w = 254 \mu\text{m}$ , maximal conversion into  $LP_{11}$  is 50%—65%, depending upon the state of the incoming polarization. This agrees well with the maximal 55% conversion from analysis of experimental intensity images.

## 5. Discussion

On the basis of theoretical simulations and experiments on mode conversion we conclude that knowing fiber and wire parameters as precisely as possible (ideally to better than a fraction of

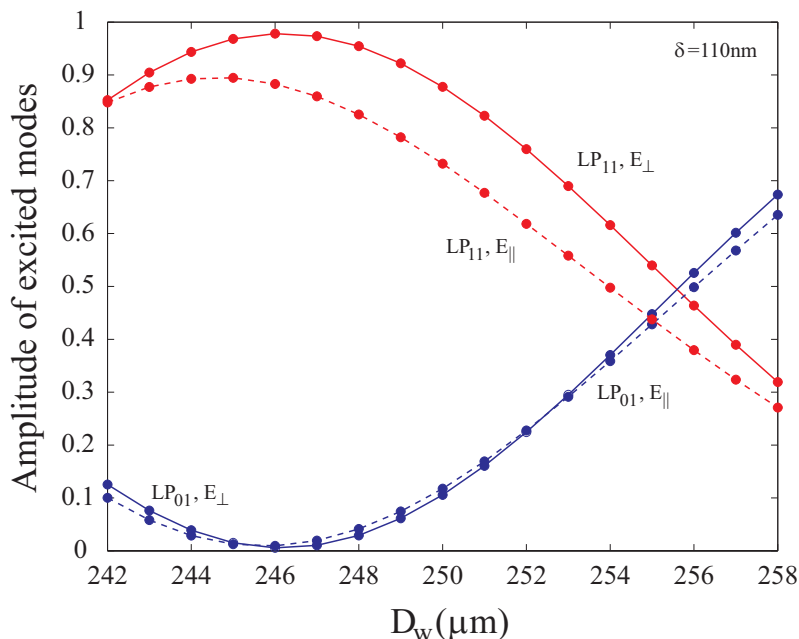


Fig. 6. Theoretical simulation of modal conversion as a function of a wire diameter in *SM* – 750 fiber undergoing  $N = 14$  consecutive bends. Fiber centerline is described by a sinusoid with an amplitude of  $\delta = 110 \text{ nm}$  and a pitch equal to the wire diameter  $D_w$ . Solid and dashed lines correspond to the perpendicular and parallel to the plane of the converter polarizations of an incoming  $LP_{01}$  mode. Upper two curves correspond to the modal weights of the higher order  $LP_{11}$  group after conversion, while lower two curves correspond to the remaining weights of the original  $LP_{01}$  mode.

a percent accuracy) is crucial in establishing a good quantitative agreement between experimental and theoretical results for “serpentine” bend converters. Particularly, from simulations in low index-contrast systems we observe that phase matching condition should be observed with better than 0.5% accuracy to achieve a 10% uncertainty in the value of the conversion amplitudes near the resonance. This translates into a sub percent accuracy in the assumed values of the fiber parameters such as fiber core radius and core-clad index contrast, and converter parameters such as wire diameter. Because of such tight tolerances, some level of tunability has to be built into the converter design to make it practical.